Highly intense lightning over the oceans: Estimated peak currents from global GLD360 observations

R. K. Said,[1] M. B. Cohen,[2] and U. S. Inan[2,3]

Received 16 January 2013; revised 7 May 2013; accepted 16 May 2013.

[1] We present the first global distribution of the average estimated peak currents in negative lightning flashes using 1 year of continuous data from the Vaisala global lightning data set GLD360. The data set, composed of 353 million flashes, was compared with the National Lightning Detection Network™ for peak current accuracy, location accuracy, and detection efficiency. The validation results demonstrated a mean (geometric mean) peak current magnitude error of 21% (6%), a median location accuracy of 2.5 km, and a relative ground flash detection efficiency of 57% averaged over all positive and negative reference flashes, and 67% for all reference flashes above 15 kA. The distribution of peak currents for negative flashes shifts to higher magnitudes over the ocean. Three case study 10°×10° regions are analyzed, in which the peak current enhancement is extremely sharp at the coastline, suggesting that the higher peak currents for oceanic lightning cannot be solely attributable to network artifacts such as detection efficiency and peak current estimation error. In these regions, the geometric mean and 95th percentile of the peak current distribution for negative cloud to ocean flashes is 22%–88% and 65%–121% higher, respectively, compared to cloud to ground flashes in nearby land regions. Globally, the majority of all negative flashes with estimated peak current magnitude above 75 kA occur over the ocean.

Citation: Said, R. K., M. B. Cohen, and U. S. Inan (2013), Highly intense lightning over the oceans: Estimated peak currents from global GLD360 observations, *J. Geophys. Res. Atmos.*, *118*, doi:10.1002/jgrd.50508.

1. Introduction

[2] It is well known that cloud-to-ground (CG) lightning flashes are a significant weather hazard. The high temperature, large and rapid charge transfer, large voltage gradient, and impulsive electromagnetic field that are associated with a CG lightning flash pose a safety risk to humans and animals [*Holle et al.*, 2005] and are well-known causes of damage to electrical systems and power transmission lines [*Kappenman and Van House*, 1996]. Airports must continuously monitor nearby thunderstorm activity in order to cease outdoor operations, especially aircraft refueling, when there is a threat of a CG strike. Space launch criteria are also limited by nearby lightning activity [*Stano et al.*, 2010; *Merceret et al.*, 2010]. Lightning location systems (LLS) are deployed around the world to monitor thunderstorm activity in order to mitigate these hazards posed by electrical activity in thunderstorms. These networks also establish large databases that can be used to investigate historical lightning patterns and parameters.

[3] The basic anatomy of a CG flash is well understood [e.g., *Uman and Krider*, 1982] and is summarized in the literature related to lightning locating systems [e.g., *Krider et al.*, 1976; *Cummins et al.*, 1998a; *Cummins and Murphy*, 2009]. The present work is concerned, in particular, with estimating the peak currents in negative first and subsequent return strokes. Using channel-base current measurements from rocket-triggered lightning experiments, *Thottappillil and Uman* [1993] have documented that a simple transmission line model of the return stroke current gives a close approximation of the radiated field during the beginning of a return stroke, i.e., up to the time of the initial peak. One consequence of this model is that at a given distance, and assuming a constant return stroke speed along a vertical channel, the peak radiated field is proportional to the peak current. This relationship has been used in many operational applications to estimate the peak current in individual return strokes [*Cummins et al.*, 1998b; *Cummins and Murphy*, 2009].

[4] The peak current is not well correlated with the total charge transferred during a return stroke. In many flashes, the currents continue to flow from the cloud to the ground between strokes, transferring the bulk of the charge over the entire flash [*Rakov and Uman*, 2003]. Nevertheless, peak current measurements are of fundamental interest, as they quantify the strength of the impulsive phase of the return stroke. The peak impulse current in a stroke likely depends

[1]Vaisala Inc., Boulder Operations, Louisville, Colorado, USA.
[2]Department of Electrical Engineering, Stanford University, Stanford, California, USA.
[3]Koc University, Istanbul, Turkey.

Corresponding author: R. K. Said, Vaisala Inc., Boulder Operations, 194 South Taylor Avenue, Louisville, CO 80027, USA. (ryan.said@vaisala.com)

2169-897X/13/10.1002/jgrd.50508

on the amount of charge deposited on the lower portion of the channel by the stepped or dart leader [*Schoene et al.*, 2010] and is used as an input parameter to over-voltage models for power transmission and distribution lines [*Nucci et al.*, 1993; *Paolone et al.*, 2009].

[5] The return strokes that follow both stepped and dart leaders generate impulsive radio waves that can be measured at long distances at frequencies from a few Hertz through to the optical band. The radio spectrum from CG return strokes peaks near 5–10 kHz, with a power spectrum that falls off inversely with frequency [*LeVine*, 1987]. The resulting radio impulses, termed radio atmospherics or, colloquially, sferics, propagate from the source, disperse, and attenuate with distance due to a finite ground conductivity and the ionosphere. Long-distance LLS operate by measuring these radio waves at multiple geographically separated sensors. Modern networks measure the arrival time and/or arrival angle of the sferics at multiple sensors and use an optimization routine that minimizes the sum of squared errors among all sensors that measured the sferic in order to geolocate the return stroke.

[6] Since the higher frequency signals attenuate faster in the Earth-ionosphere waveguide, long-range networks, which are capable of detecting lightning flashes >1000 km from each sensor, operate in the very low frequency (VLF; 3–30 kHz) range. Precision networks measure higher frequency content in the low frequency (LF; 30–300 kHz) band or higher to improve timing and therefore location accuracy but are limited by operating sensor ranges of a few hundreds of kilometers. One network that has been operating continuously in the U.S. for over 20 years is the National Lightning Detection Network™ (NLDN) [*Krider et al.*, 1976; *Cummins and Murphy*, 2009]. This network uses a combination of arrival azimuth and arrival time measurements to compute geolocations using two or more sensors. Since it relies on VLF/LF measurements to obtain accurate arrival time information, the operating range of the network is limited to a few hundred kilometers from the network's boundary, roughly defined by the U.S. coastline. The NLDN currently detects ~90%–95% of CG flashes according to model estimates [*Cummins and Murphy*, 2009]. Using data from rocket-triggered lightning experiments as ground truth, *Nag et al.* [2011] reported a 92% NLDN ground flash detection efficiency (DE) and a median location error of 308 m. A recent deployment of propagation corrections has improved the location accuracy to ~250 m [*Cummins et al.*, 2010].

[7] Establishing global patterns of the estimated peak current is relevant both for storm dynamics and safety. Several lightning climatology studies that use data from the NLDN have shown contour maps of the average peak current estimates. In a study of the climatology of large peak current events over the U.S. from summer months between 1991 and 1995, *Lyons et al.* [1998] noted an increase in the relative occurrence of very intense (>75 kA) negative strokes in the Gulf of Mexico and off of the southeastern U.S. coastline. The observed enhancement generally follows the coastline, with a soft boundary along the eastern U.S. coastline and some of the enhancement seen over land on the Gulf boundary. The authors postulated that the high conductivity of the salt water was responsible for this increase, though they could not explain the higher peak currents as much as 100 km inland from the Gulf of Mexico.

[8] Using a decade of NLDN data, from 1989 to 1998, *Orville and Huffines* [2001] confirmed the observation that peak current magnitudes increase on average over the ocean for negative CG flashes. Median peak currents jumped from ~27 kA to >30 kA along much of the Gulf coast and eastern U.S. coastline. The same soft boundary is seen in parts of the Gulf coast and the eastern coast of Florida and the northeastern coast of the U.S. In contrast to negative cloud to ground/ocean flashes, median peak currents from positive flashes did not show an increase across the land-sea boundary. In a follow-up study using NLDN data from 2001 to 2009, *Orville et al.* [2011] reported very similar results, showing no enhancement over the Great Lakes, and a relatively sharp enhancement in median negative oceanic lightning peak currents, beyond what one would expect from network effects alone. No similar enhancement was seen in positive flash data.

[9] Instead of an actual increase in peak current, *Cummins et al.* [2005] argue that it is more likely that only the peak field, which is used by LLS to infer peak current, is enhanced due to the specifics of the attachment process between a negative stepped leader and salt water. Most previous observations and theoretical formulations of the attachment process focus on strikes to grounded structures [*Berger*, 1967; *Cooray and Theethayi*, 2007], though video observations of natural lightning have shown that upward connecting leaders induced by stepped leaders that precede new ground contact points are much longer (tens of meters) than those induced by dart leaders in subsequent strokes [*Orville and Idone*, 1982]. *Cummins et al.* [2005] specifically investigated the relationship to the leader type of the observed enhancement of oceanic lightning peak currents by comparing thematic averaged peak current maps in the Southeast U.S. and surrounding oceanic regions for four classes of events: positive first strokes, positive subsequent strokes, negative first strokes, and negative subsequent strokes. The enhanced peak current was only observed for negative first strokes (roughly 25% increase across the land-sea boundary), leading the authors to suggest that the effect is due to the properties of the attachment process for negative stepped leaders over a smooth, highly conducting surface. While the low surge impedance of salt water could interact in some preferential way with the impedance of negative stepped leader channels, they suggest two other mechanisms that could enhance the peak field without increasing the peak current. An increased return stroke velocity resulting from either the surge impedance of salt water or by an enhancement of the electric field due to reduced boundary layer screening would lead to a larger peak field for a given peak current, according to the transmission line model used to relate peak currents to the measured field. The second proposed mechanism stems from E and dE/dt measurements of first cloud-to-ocean strokes reported by *Murray et al.* [2005]. The authors found that 37% of first return strokes had at least one dE/dt pulse within 1 μs of the dominant peak. The median peak E-field from these events was 38% larger than strokes with only one dE/dt pulse due to the integrated effect of multiple dE/dt pulses. The authors suggested the multiple dE/dt pulses could be due to multiple branches in the last leader step or upward connecting discharges. It is unclear if

a similarly complicated attachment process occurs over land or over poorly conducting freshwater.

[10] *Tyahla and Lopez* [1994] investigated the peak current distribution in two small (60 km) coastal regions near the Kennedy Space Center in Florida where the triggering biases were minimal. The authors did not notice more intense field changes from sea lightning, indicating that the transition may be more gradual in some regions like Florida, consistent with *Orville and Huffines* [2001].

[11] These past studies of peak current distributions using NLDN data were limited by the geographic extent of the network. *Füllekrug et al.* [2002] investigated very intense lightning on a global scale using a network of three magnetometers sensitive to extremely low frequency (ELF) waves and found that the majority of negative return strokes with large charge moments (–6 kC · km to –2 kC · km) occurred over the oceans. Global lightning climatologies have also been based on satellite measurements, such as the global lightning flash density map produced by *Christian et al.* [2003] using satellite-based optical measurements. This experiment provided the first estimate of global lightning flash rate distribution using a systematic sampling of in-cloud and cloud-to-ground flash data, but it did not attempt to estimate peak current values for individual return strokes. *Christian et al.* [2003] did find that total flash occurrence is roughly an order of magnitude higher over land compared to ocean.

[12] Evidence for a larger relative population of high peak current flashes over the ocean has been reported using Elve counts detected by the Imager of Sprites and Upper Atmosphere Lightning (ISUAL) sensor on the FORMOSAT-2 satellite as a proxy measurement [*Chen et al.*, 2008]. The ISUAL sensor measured optical signatures of various transient luminous events, including Elves, which are optical emissions at altitudes of 75–95 km produced by heating and ionization from the VLF electromagnetic pulse generated by lightning return strokes [*Inan et al.*, 1991; *Fukunishi et al.*, 1996; *Inan et al.*, 1997]. The occurrence of Elves is correlated with the LLS-reported peak current of individual return strokes: *Barrington-Leigh and Inan* [1999] observed Elves for all ground flashes with peak currents larger than 57 kA but reported a much lower incidence for weaker flashes. Thus, a global survey of Elves can serve as a proxy for a global climatology of large (>60 kA) peak current flashes. From the ISUAL data, *Chen et al.* [2008] reported a land-to-ocean ratio of 1.1:1 for Elves. Since there is a $\sim$10:1 ratio of land to oceanic lightning, this result infers that the relative occurrence of Elves, and therefore of large peak current flashes, is much higher over the ocean.

[13] In this paper, we use data from the global lightning data set GLD360, which is generated by a long-range LLS network owned and operated by Vaisala, to study negative first-stroke peak current distributions on a global scale. Previous validation studies have put the median location accuracy at 2–5 km and the CG flash DE at $\sim$70% [*Poelman et al.*, 2013; *Pohjola and Mäkelä*, 2013], which is exceptionally good for a global LLS. GLD360 is also the first global LLS to estimate peak current for all detected individual return strokes, though the source type (cloud pulses versus return strokes) is not reported. The global reach of GLD360, coupled with its ability to report peak current values across the entire domain of the network, provides a unique data set for investigating peak current distributions across multiple regions of the world. We present below the first observations of lightning peak current measurements on a global scale based on a year of lightning geolocation data from the GLD360 data set.

[14] Section 2 begins with a detailed description of GLD360, its approach to estimating peak current values, and a validation of the peak current values and location accuracy using NLDN data as a reference. The data processing used to display data in thematic maps is also discussed. Section 3 presents summary statistics and distributions of GLD360-determined peak current values and focuses on three regions to highlight land-sea peak current differences. Section 4 discusses the results in the context of the network's performance limitations.

2. Measurements and Display Methods

[15] The methodology of GLD360 is detailed in *Said et al.* [2010]. Each sensor stores a local empirical waveform bank, which catalogs the expected sferic waveform shape, indexed by distance and ionospheric profile. The empirical waveform bank was derived using a VLF receiver and known lightning location data from NLDN. The most reliably repetitive features (either the rising portion of the ground wave or the zero-crossing of the first or second ionospheric reflection) are used to establish the precise arrival time of the sferic at the receiver. Finally, the arrival angle is determined [*Said et al.*, 2010]. This information is sent back to a central processor, which then aggregates arrival time data to make a determination of the event's time and location using an optimization routine that minimizes the squared error of all time and azimuth measurements. The network also measures the polarity of each stroke via the cross correlation with the waveform bank. An event must be simultaneously detected by at least three sensors to be geolocated, though most are detected by more.

[16] Each sensor measures the peak magnitude of the magnetic field, which is used by the central processor to estimate the peak current of each event. Since GLD360 was designed for uniform coverage across the globe from land-based sensors, detection ranges of thousands of kilometers are necessary; hence, its sensors are sensitive to the VLF frequency band [*Cohen et al.*, 2010]. After geolocation, the peak magnitudes are corrected by the source-receiver distance using a propagation model and then converted to a peak current value using a conversion coefficient [*Said et al.*, 2010]. Since the magnetic field, rather than electric field, is used to measure the sferic, each sensor is less susceptible to field enhancements due to local terrain and ground electrical conductivity. The peak current estimate of the detected event is calculated by taking a weighted average of the estimates from each sensor contributing to the geolocation solution. To mitigate the effects of saturation at any given receiver for very large events, sensor reports that are near saturation are down-weighted compared to sensor measurements with amplitudes that are well within the dynamic range limits of the sensor. While GLD360 does not currently distinguish between ground and cloud flashes, propagation-adjusted VLF peak values (measured in picoteslas) are used to assign an effective peak current to each event, referenced to NLDN CG strokes.

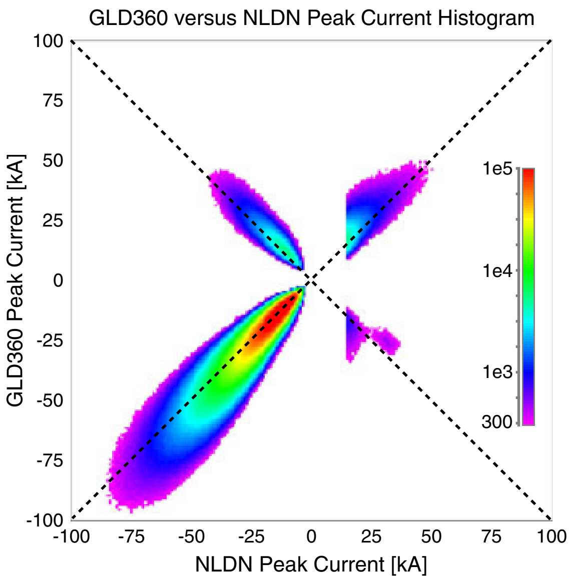

Figure 1. Two-dimensional histogram of GLD360-reported peak currents versus NLDN-reported peak currents for events matched over the U.S. between 21 July 2011 and 21 July 2012. The color scale indicates the number of matched events in each 1 kA × 1 kA bin. Slope ±1 lines are drawn for reference. Bins with fewer than 300 matched events are omitted.

[17] Validating peak current reports of naturally occurring CG strokes is a challenging task. A structure or tower can be equipped with current measurement devices, but the metallic structure itself alters the electrical properties of the upward leaders and attachment process [*Bazelyan and Chichinskiy*, 2009]. Another approach uses channel-base current measurements from rocket-triggered lightning. The phenomenology of a rocket-triggered stroke is similar to that of a natural stroke following a dart leader, so this technique does not necessarily validate peak current reports of strokes following a stepped leader, including first strokes and subsequent strokes forming new ground contact points. A recent validation study comparing 5 years of rocket-triggered lightning data to geolocated NLDN events found an arithmetic mean (median) magnitude error of 17% (13%) [*Nag et al.*, 2011].

[18] For VLF sensors, the validity of the transmission line model begins to break down due to the increasing wavelength size with respect to the channel length. Furthermore, beyond ~700 km, the peak field amplitude of the received waveform is received from ionospheric reflections rather than the ground wave. Nevertheless, *Said et al.* [2010] showed a strong correlation between inferred peak current values using VLF measurements and those reported by the medium-range NLDN. A linear relationship between the peak currents reported by NLDN and the measured peak VLF amplitude was shown, where approximately two thirds of the events were within a factor of 1.69 of the average value.

[19] An expanded validation of GLD360's peak current values is presented here, using NLDN values over a large portion of the U.S. and over a much longer time window. The NLDN is chosen due to its convenience and provides a large coverage area with near-uniform precision network-quality performance. While this comparison only validates GLD360's peak current performance over the U.S., the same propagation parameters are applied in other regions of the globe. Figure 1 shows a 2-D histogram of peak current values for events matched to NLDN ground strokes using 1 kA × 1 kA bins. A time-space coincident window of 150 μs and 50 km, respectively, was used to match events between the two data sets, over a common latitude/longitude bound of [25, 55], [–125, –70]. With perfect correlation between the two data sets, the histogram would lie entirely on the dotted +1 slope line. Correlated events in the quadrants occupied by the –1 slope line indicate events where the two networks measured opposite polarities. NLDN classifies all positive events with peak current <15 kA as cloud pulses, so there is a gap for small positive events.

[20] Figure 2 quantifies the mean, geometric mean, and percent polarity agreements versus peak current between the two networks. Averaged across all peak current values, the two networks measured the same polarity for 96% of matched strokes. The overall geometric (arithmetic) peak current magnitude error is 6% (21)%. Since these errors are in reference to NLDN strokes, we multiply (add) these values to the median (mean) of the NLDN peak current errors from *Nag et al.* [2011] to obtain a worst-case magnitude geometric (arithmetic) mean error of 20% (38%). Since peak current values roughly follow a log-normal distribution [*Berger*, 1975], so do the peak current errors, and so the unreported geometric mean of the NLDN peak current error distribution should approximately equal the median. We reiterate that these estimates are only validated for subsequent strokes in negative CG flashes.

[21] The relative peak current performance metrics degrade for weak reference events. The steep increase of the mean compared to the geometric mean of the magnitude error for these weak events suggests a small population of relatively large magnitude error events, though the small reference peak current leads to a large relative error for even modest absolute magnitude peak current errors. The decreased performance for these weak events may be due to a lower signal to noise ratio and likely due to some mixing with misclassified cloud pulses or miscorrelated stepped leaders.

[22] Figure 3 validates GLD360's location accuracy over the same latitude/longitude and time window used above. This plot shows the histogram and cumulative distribution function (CDF) for the collection of relative distances between matched GLD360 events and NLDN strokes. The median (90th percentile) location accuracy is ~2.5 (17.5) km. The secondary hump near 11 km error is due to "two-cycle" errors and GLD360's current limitations to correct for mixed day-night paths [*Said et al.*, 2010]. The majority of events are located within a typical storm cell size, and thus, the extent of the thunderstorm activity is well captured by the network.

[23] Another important metric for a LLS is the detection efficiency, which can be defined in multiple ways. Using the NLDN network as a reference, we investigate here the relative ground flash detection efficiency—the percentage of NLDN-recorded ground flashes that had at least one constituent stroke matched to a GLD360 event using the time

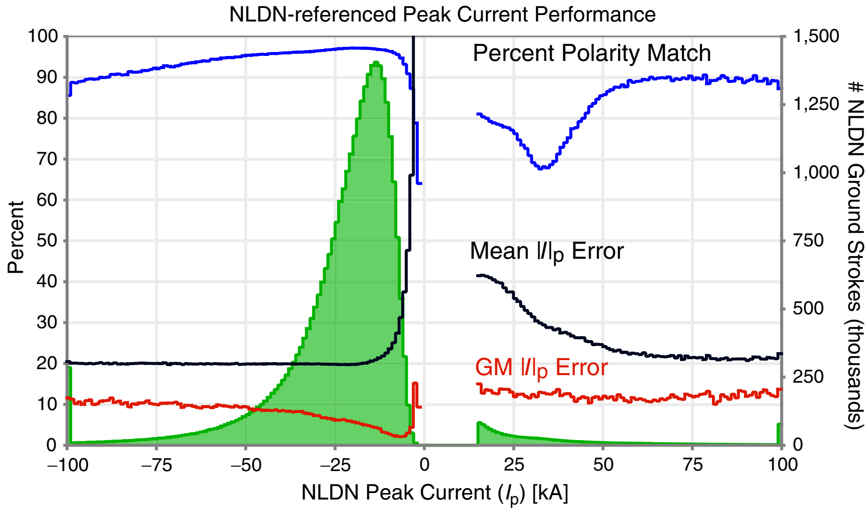

Figure 2. Quantification of the peak current performance from the data plotted in Figure 1, calculated for each 1 kA bin. The filled histogram shows the number of matched events. The blue, black, and red curves plot the percent matched events with the same polarity, and the mean and geometric mean of the peak current magnitude error as a percentage, respectively.

and space match window above. This metric does not give an overall flash detection efficiency, since it excludes cloud flashes. We also do not adjust the values for the absolute ground flash DE of NLDN. Averaged over all flashes for the 1 year period beginning 21 July 2011, and using the latitude and longitude bounds given above, GLD360's relative ground flash DE was 57%. For NLDN flashes with a peak current magnitude (determined by the first stroke in the flash) over 15 kA, the relative DE was 67%. Over the U.S., there are several key sensors in the GLD360 network that are responsible for providing coverage to that region. If we filter out days where at least one of these sensors was unavailable for the entire day, which was 25% of all calendar days during this time span, the relative DE jumps to 63% over all peak current ranges, and 72% for flashes with peak current magnitude over 15 kA.

[24] Section 3 presents several thematic maps with flash densities and the geometric mean (GM) and 95th percentiles of estimated peak current values. The percentile values are calculated using the "P^2-Algorithm," a constant-memory technique for estimating quantiles [*Jain and Chlamtac*, 1985]. Since peak current magnitudes typically follow a log-normal distribution, the geometric mean is the appropriate metric to capture the average of the distribution. The 95th percentile estimate characterizes the upper tail of the distribution. Since only 1 year of data was used, grid sizes of 0.5° × 0.5° (Figures 4-6) and 0.25° × 0.25° (Figure 8) were used to ensure sufficient statistics in each pixel. In order to aid in the visual identification of contour lines and to filter out high spatial frequency variations due to the limited sample size, the geospatial data were spatially upsampled using nearest-neighbor interpolation [*Lehmann et al.*, 1999] and then convolved with a Gaussian kernel

$$G(i,j) = \left(2\pi\sigma^2\right)^{-1} \exp\left[-(i^2+j^2)/(2\sigma^2)\right]$$

[*Kisacanin et al.*, 2009, pp. 104]. Attributing a characteristic width to the convolution filter of $\sim 2\pi\sigma$ pixels, which is the inverse of the standard deviation of the Fourier Transform of G, the spatial resolution of the resulting image with original pixel width D ($\sim$55 km for Figures 4–6 and $\sim$27 km for Figure8) that has been upsampled by a factor of N and convolved with G is $\sim D(2\pi\sigma/N)$. Assuming square pixels, which is approximately true for subtropical and tropical latitudes, and with $N = 6$ and $\sigma = 1.91$, the minimum discernible feature size is $\sim 2D$. The net effect is the ability to visually inspect contour lines coupled with the ability to discern gradients within each color range. These filter coefficients are used in all thematic maps below.

3. Results

[25] This section presents a series of thematic maps and statistical results from GLD360 flash incidence and peak current data over a 1 year period, from 21 July 2011 through 21 July 2012. Over this period, GLD360 detected 353 million flashes across the globe, which averages to 11.2 flashes/s. Assuming an average $\sim$3:1 ratio of cloud flashes to ground flashes [*Prentice and MacKerras*, 1977; *Boccippio et al.*, 2001] and if GLD360's ground flash detection efficiency

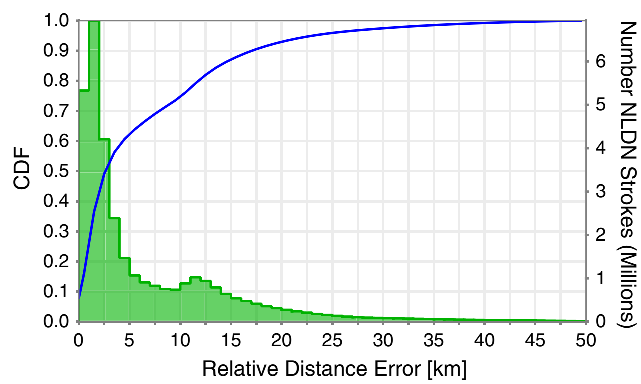

Figure 3. Histogram and cumulative distribution function of the relative distance error between matched GLD360 events to NLDN ground strokes, using data from 21 July 2011 to 21 July 2012.

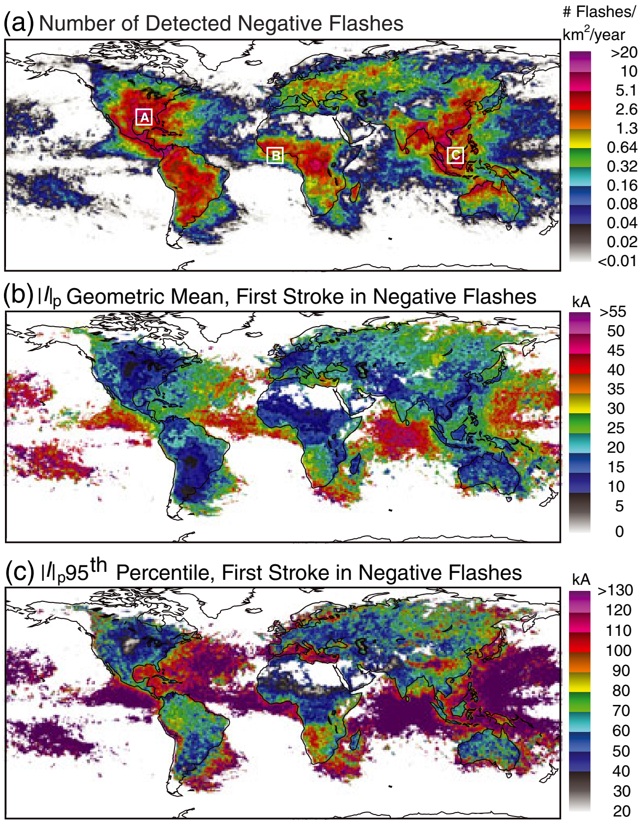

Figure 4. (a) Number of events, (b) peak current magnitude geometric mean, and (c) peak current magnitude 95th percentile of all first negative events from flashes detected by GLD360. Each plot is constructed with 0.5° × 0.5° bins that have been upsampled by a factor of 6 and smoothed using a Gaussian filter with σ = 1.91, giving approximate spatial resolution of 1.0°. Each of the 11 color ranges in Figure 4a, including the dark and light gray regions, marks a factor of 2 increase in the average detected flash density. The lowest gray box captures regions with flash densities down to 0.004 flashes · km^{-2} · yr^{-1}; regions with lower flash densities are not shown. The color ranges in Figures 4b and 4c mark 5 kA and 10 kA increments, respectively. The segmented color scale is chosen to highlight contour lines. Regions with fewer than 0.02 flashes · km^{-2} · yr^{-1} are omitted in Figures 4b and 4c. The bounding boxes in Figure 4a indicate regions A, B, and C in Figure 8.

is much higher than its cloud flash detection efficiency, this figure is consistent with the ~45 flashes/s reported by *Christian et al.* [2003]. Since the source type (CG versus cloud pulse) is unknown, all detected events were treated as possible ground strokes. All events were first clustered into flashes, using the same grouping algorithm detailed in *Cummins et al.* [1998b], but with a 20 km coincidence window to accommodate a larger tail in location errors from the lower precision data set. Each constituent stroke in the clustered flashes was then identified by its stroke order, starting with one for the first identified event in the flash.

[26] Figure 4a shows the number of negative flashes detected by GLD360 per square kilometer over the 1 year period. The flash density values have not been corrected for DE. Since the values are uncalibrated, and since all positive flashes (which include many cloud events) have been filtered out of the data set, this figure is not meant to establish a global lightning rate climatology, as was done using 5 years of satellite observations in *Christian et al.* [2003]. Nevertheless, many features from the satellite-based global lightning distribution seen in Figure 4 of *Christian et al.* [2003] are readily apparent. Flash densities are generally higher over land due to greater vertical instability caused by diurnal heating of the terrestrial landmasses. The Southeast U.S., central Africa, and Southeast Asia are global hot spots of lightning, along with significant activity in Central and South America. Much of the fine structure of previously reported global flash density rates are also reproduced in this plot.

[27] The next two panels in Figure 4 show the geometric mean and 95th percentile of estimated peak current magnitudes of the first detected events in negative flashes. As with Figure 4a, these results have not been corrected for DE. Over large portions of the ocean, the GM is over 35 kA. This skew to higher magnitudes is partially due to a lower DE over the oceans where the average sensor density drops, since at least three sensors are needed to geolocate a lightning event. Each sensor has a minimum detectable amplitude threshold dictated by the local noise profile. As the distance from a region to the closest three sensors increases and thus the attenuation

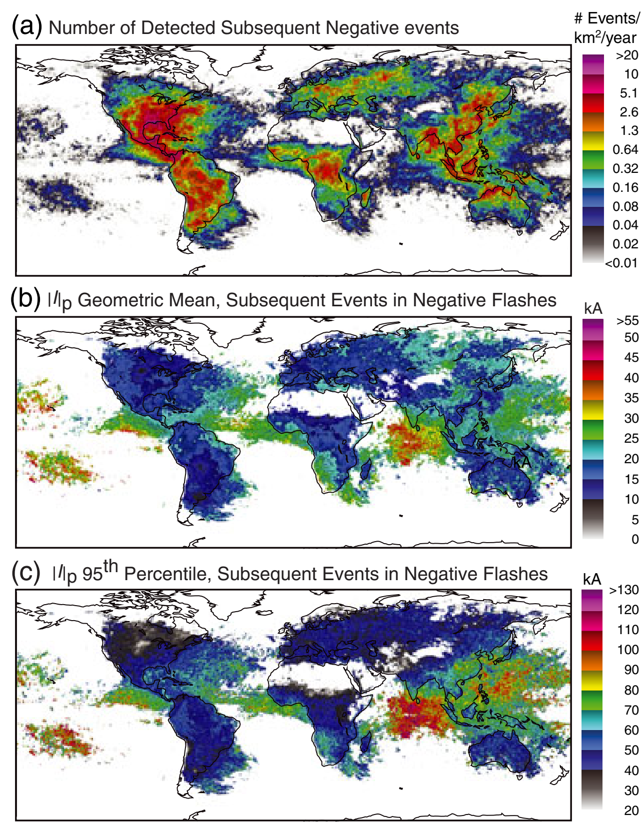

Figure 5. (a) Number of events, (b) peak current magnitude geometric mean, and (c) peak current magnitude 95th percentile of all subsequent negative events from flashes detected by GLD360. The color ranges are the same as in Figure 4.

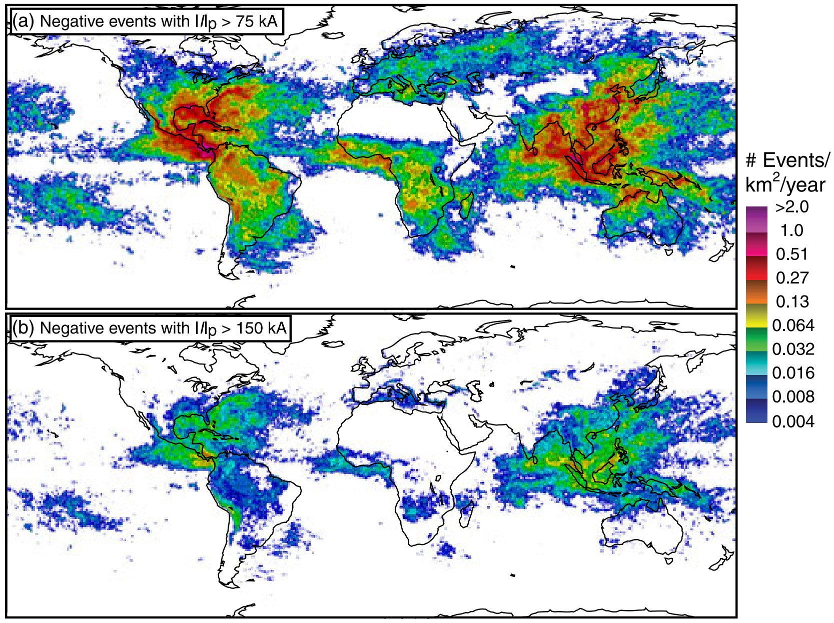

Figure 6. Number of negative events (first and subsequent strokes) with detected peak current magnitude (top) above 75 kA and (bottom) 150 kA. The same bin size and processing parameters from Figure 4 are applied here. Regions with event densities below 0.004 events $\cdot$ km^{-2} $\cdot$ yr^{-1} are not shown.

from the source of the detected sferics increases, the distribution of detected peak currents skew toward more powerful (higher peak current) events. Nevertheless, it is clear from the GM plot and, to a much greater extent, the 95th percentile plot that the peak current magnitude distribution skews toward higher peak current values over the oceans, with sharp gradients along several of the coastlines. The freshwater Great Lakes in the U.S. show no noticeable peak current enhancement. The Black and Caspian seas display a modest enhancement over the immediately surrounding land areas.

[28] Figure 5 shows the corresponding global thematic maps for subsequent strokes in negative flashes. The land-sea boundaries for these subsequent stroke currents are less pronounced. Nevertheless, there is still a noticeable enhancement across many land-sea boundaries, including along the western Mexican and Central American coastline, along western Africa, and along several coastlines in Southeast Asia.

[29] Figure 6 plots the total count density of all GLD360-detected events over 75 and 150 kA. Contrasting this plot with the flash densities shown in Figure 4a, it is clear that the high peak current regions are disproportionally distributed over the oceans. Large portions of the U.S., South America, and Africa have relatively high annual flash rates but comparatively low absolute numbers of very high peak current events. The high flash rates in Southeast Asia also produce a high density of large peak current events, but the distribution of high peak current events is visibly skewed to the oceanic and coastal areas. The two highest active regions for very large peak current events are centered off the eastern and western shores of Costa Rica and Panama, and in the Malacca straight in Malaysia. The distribution of high peak current events is consistent with the distribution of Elves measured by the ISUAL experiment. *Chen et al.* [2008] show high Elve rates in these same two regions, along with other regions in Southeast Asia and Papua New Guinea that also have a high occurrence of large peak current events.

[30] Figure 7 shows a distribution of global peak current estimates for the entire year and the ratio of these distribu-

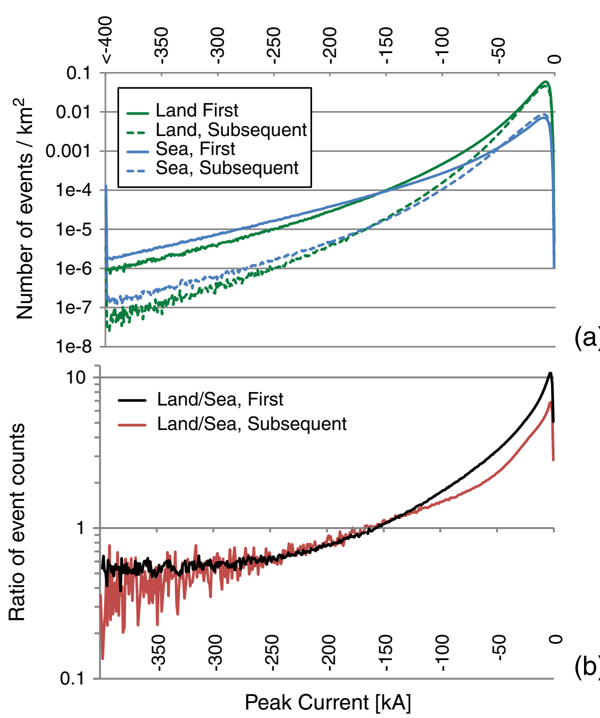

Figure 7. (a) Normalized distribution of global peak current values over land and sea between –50°N to 50°N, using 1 kA peak current bins. (b) Ratio of global land:sea distributions for first and subsequent strokes.

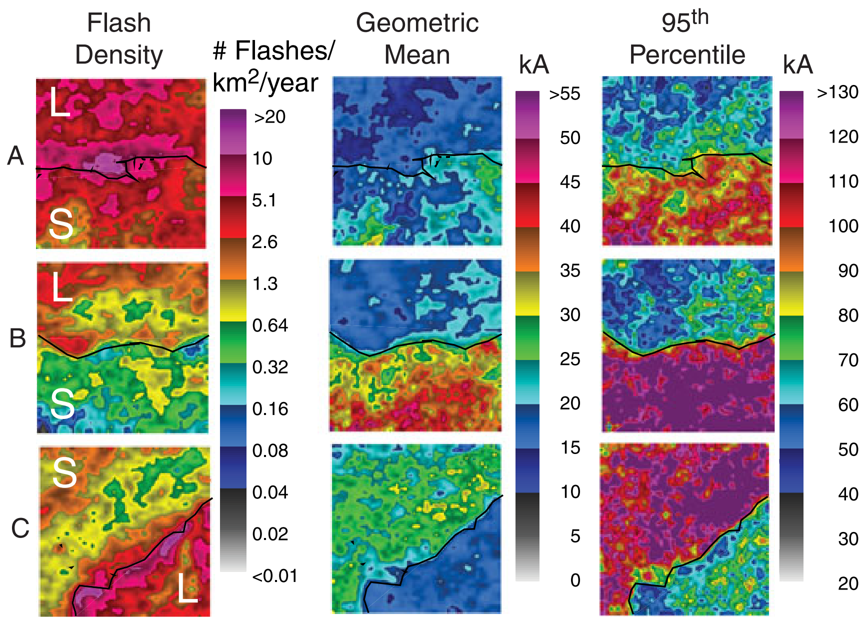

Figure 8. Thematic plots from three regions highlighted in Figure 4, with 0.25° × 0.25° bins that have been upsampled by a factor of 6 and smoothed using a Gaussian filter with σ = 1.91, giving approximate spatial resolution of 0.5°. First column shows flash density for regions A, B, and C, corresponding to latitude and longitude ranges [25, 35], [–95, –85]; [0, 10], [–10, 0]; and [0, 10], [107, 117] degrees, respectively. Each 10° × 10° window contains a coastline boundary. The side labeled with an "L" indicates the land region, and the side with an "S" indicates the oceanic region. Second column (third column) shows geometric mean (95th percentile) of the peak current magnitude from first strokes in negative flashes for regions A, B, and C.

tions for each peak current bin. The distributions have been normalized by the total land and sea area resulting in equal area density values, and the data were limited to ±50° to minimize the effects of a decreasing DE at extreme latitudes. Both the land and oceanic distributions peak near 10 kA, but the high peak current tail of the oceanic distribution curve falls off at a slower rate than the tail of the corresponding land distribution. The drop in counts for peak current magnitudes below 10 kA is due both to a true drop in the CG peak current distribution and a decreasing DE for weak CG strokes and cloud pulses. The relative enhancement of the estimated peak current in oceanic lightning compared to lightning over land is consistent with the larger enhancement seen in the 95th percentile plots as compared to the GM plots of estimated peak current in Figures 4 and 5. The ratio of normalized global land to sea counts (Figure 7b) peaks at ∼10 for weak (∼10 kA) events. In the high peak current tails, the oceanic distribution crosses over the land distribution at ∼150 kA. For peak current events above 300 kA, the normalized occurrence density over the ocean is twice that detected over land. On this global scale, a similar enhancement of large oceanic peak current events is seen for subsequent strokes.

[31] Without normalizing by land/sea area, the crossover to higher absolute counts of oceanic events occurs at lower peak current magnitudes. For first (subsequent) strokes, there are more oceanic lightning events globally with estimated peak currents above 75 (51) kA than land events. For both first and subsequent strokes, there are twice as many global oceanic lightning events with estimated peak currents above 140 kA than land events. Given the 10:1 occurrence of land to oceanic lightning globally, these results emphasize the skew toward larger values in the oceanic negative lightning peak current distribution.

[32] In an effort to remove bias due to a drop in detection efficiency in the more remote oceanic areas, three regions were isolated and analyzed separately. These three regions, indicated by boxes A, B, and C in Figure 4a, cover 10° × 10° boxes, with a land:sea partition roughly bisecting each bounding box. Figure 8 shows enlarged views of these three boxes for each plot, but with double the spatial resolution.

[33] Region A is the Southern U.S. interface to the Gulf of Mexico. In this region, there is a minimal dropoff in flash density across the land-sea boundary. The peak current magnitude GM shows a slight enhancement over the ocean, particularly in the eastern half of the region. The increase in the GM in the southwest corner is spatially coincident with a decrease in flash density, so it is unclear if this enhancement is physical or due to a drop in DE. The 95th percentile plot shows a more dramatic average increase in values over the gulf. The separation between the 95th percentile values on the land and sea side of the coastline is not complete. Nevertheless, there are only small pockets over the land with a peak current 95th percentile value above 80 kA, and the majority of distributions over the ocean have a value higher than this level. Also, the contours to larger (>80 kA) 95th percentile values span ∼100 km on either side of the coastline, which is consistent with the soft boundary to larger peak current averages noted in earlier studies. The modest increase in the GM, contrasted with the larger increase in the 95th percentile, indicates that the tail of the peak

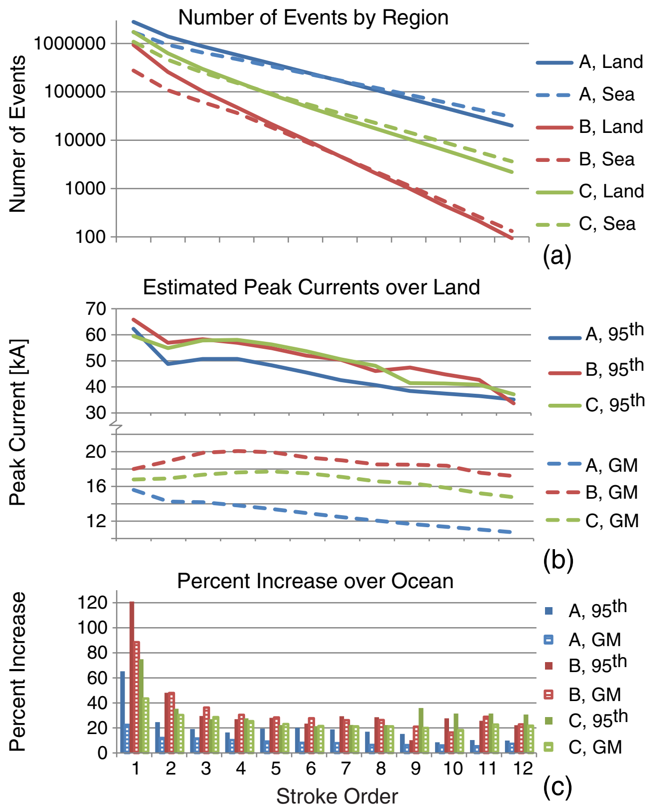

Figure 9. Peak current distribution parameters for regions A–C indexed by stroke order. (a) Number of detected events over land and sea. (b) Geometric mean and 95th percentile of measured peak current magnitudes over land. (c) Percent increase in geometric mean and 95th percentiles of the peak current distribution for events detected over the ocean versus those detected over land.

current magnitude distribution is shifted more dramatically compared to the center of the distribution.

[34] Region B encompasses the southern coastline of Western Africa. In this region, the flash density shows an overall drop over the ocean, though there are some regions over the ocean that have the same average flash density as over land. The sharp gradient in flash rates along the coastline suggests that this drop is not due to a gradient in DE. As with region A, the 95th percentile values increase over the ocean, but the gradients to higher values follow the coastline much more closely. In contrast to region A, the GM also increases by a substantial amount over the ocean, with a transition to higher values closely following the entire coastline. Over most of the domain, the GM increases by ∼15 kA over the ocean, and the 95th percentile increases by ∼40–50 kA. The separation of the peak current distributions between the oceanic region and the terrestrial region is nearly complete: Most of the oceanic region shows a GM (95th percentile) over 30 kA (130 kA), and all oceanic regions are above 25 kA (100 kA). Over land, most of the region has a peak current GM (95th percentile) below 20 kA (80 kA), and all land areas are less than 25 kA (100 kA).

[35] Region C covers the northwest region of Borneo and the South China Sea. This region shows a more diffuse flash rate boundary on the coastline, and the flash rate increases again in the northwest corner (over the ocean) of the analysis window. In contrast, the GM and 95th percentile values of the peak current distributions increase sharply along the coastline, similar to the sharp increase in region B.

[36] We now investigate the dependence of this observed enhancement in the peak current distribution on stroke order for negative flashes over the ocean. Figure 9 shows accumulated statistics partitioned by stroke order over both the terrestrial and oceanic areas from regions A, B, and C. Figure 9a shows the distribution of detected events. In all three regions, there were more flashes (first strokes) detected over land, as is meteorologically expected and as is apparent from the first column in Figure 8. Also, the slope of the event count distributions with respect to stroke order is lower over the ocean. It is unclear if this result is due to a true change in stroke order distribution over the ocean, better DE in these regions due to propagation over salt water, or a higher incidence of large cloud pulses that are interpreted as strokes in the same flash. Figure 9b shows the 95th percentile and the GM of the measured peak current magnitude for events over land. The lower peak current distribution in region A may be due to a higher DE in that region compared to regions B and C. Figure 9c shows the percent increase in the GM and 95th percentiles of the peak current distributions for oceanic lightning compared to terrestrial lightning in regions A–C. In all three cases, the relative increase in both metrics was greatest for the first detected event in the flash. In region A, the 95th percentile (GM) increases over the ocean dropped from 65% (22%) to 25% (12%) between the first and second detected strokes. Region B showed the largest increase in the 95th percentile (GM) over the ocean of 121% (88%). The increase over the ocean dropped to 48% for both metrics for the second stroke. Region C had the lowest percentage drops between the first and second stroke, from a 95th percentile (GM) of 75% (43%) to 35% (30%).

4. Discussion and Conclusions

[37] Our results show for the first time that the observed enhancement of negative estimated peak currents seen near the U.S. coastline is a global phenomenon. Since earlier observations of this enhancement relied on continental scale networks, it is possible that previous results were in part due to network effects. Using 1 year of data from the long-range GLD360 data set, which we compared to the NLDN network over the same time period, we demonstrated that this peak current enhancement is not due to network effects alone. Further research into the differences between the attachment processes in terrestrial and oceanic lightning is needed to determine the cause of this enhancement.

[38] As mentioned above, the observed peak current distribution in a given region is the result of the true peak current and the network's detection efficiency as a function of that current. A distribution skewed toward higher values, therefore, may be due to a decrease in DE for lower peak current events. This paper does not introduce a normalization factor to account for such a decrease in DE. Thus, the higher GM and 95th percentile of the observed peak current in the interior of the oceans may be in part due to a decrease in DE. However, in such a long-range network, there is no network-intrinsic or otherwise physical reason for a large

change in DE at a land-sea boundary. Also, the average sensor baselines are several times longer than the width of the analysis windows, and so differential propagation effects should not change as drastically. We conclude, therefore, that the observed enhancement of the signals from negative flashes over the oceans is a real physical phenomenon. Furthermore, for very large events, the DE is more uniform, and so the distribution of very large peak current events shown in Figures 6 and 7 is not likely to be greatly affected by this unequal DE.

[39] We reiterate that the peak current calibration for first strokes is less certain than for subsequent strokes in existing channels, so the absolute values reported here for the peak current of first detected strokes may be less accurate. Strokes preceded by stepped leaders have different attachment and return stroke dynamics [*Borghetti et al.*, 2003; *Bazelyan and Chichinskiy*, 2009], and so the empirical correction factor derived for the NLDN from rocket-triggered experiments and, by extension, GLD360, do not necessarily translate to actual peak currents of first strokes. Furthermore, peak current estimates for NLDN have only been validated for subsequent strokes with peak current magnitudes less than ∼45 kA [*Jerauld et al.*, 2005; *Nag et al.*, 2011], and linearity is assumed for strokes with a larger peak current. Nevertheless, regardless of the true calibration factor, these results demonstrate a relative enhancement of radiated field from first strokes in negative oceanic lightning as compared to terrestrial lightning.

[40] In general, we expect that the lack of knowing the specific type of stroke will weaken the difference between peak current distributions for terrestrial and oceanic regions. Without better event type classification, the average peak current, calculated using the range-normalized peak magnetic field values, will mix measurements of CG strokes and cloud pulses. However, since cloud pulses generate lower amplitudes in the VLF band on average [*Cummins and Murphy*, 2009] and the land-sea differences are not expected to play a major role for cloud pulses, the inclusion of cloud pulses in our results should only weaken the difference between the distributions of oceanic and land sources. For example, a higher cloud DE in region A may partially explain the lack of increase in the GM over the ocean relative to the enhancement seen in regions B and C. We have mitigated this mixing effect by filtering out all positive events: Small positive events are much more likely to correspond to cloud pulses, and so this filtering preferentially isolates CG strokes.

[41] The results presented herein are consistent, though not as dramatic, as the lack of enhancement in subsequent strokes in the same channel shown in *Cummins et al.* [2005]. Figure 9 shows a sharp decrease, on the order of 55%-60%, of the 95th percentile in the peak current magnitude distribution over the oceans between the first detected event and all subsequent events. The GM drop was more modest, ranging from 30% to 45% across the three regions, which is consistent with our observation that the tail of the distribution is enhanced more over the oceans than the center of the distribution. Since GLD360 does not distinguish between CG and cloud pulses, some of the first strokes may be misclassified cloud pulses. It is also possible that these higher peak current events consist of subsequent strokes that form new oceanic contact points, particularly if the apparent increase in peak current is due to the attachment mechanism of negative stepped leaders. Using video recordings of 39 negative CG flashes over land and stroke data from the NLDN, *Stall et al.* [2009] found that 48% of all subsequent strokes formed new ground contacts (NGC). Of all observed strokes forming NGC, 59% had stroke order 2, and another 27% had stroke order 3. This pattern of NGC incidence versus stroke order is qualitatively similar to the decrease in the percent increase of the GM over the ocean for stroke orders 2 and 3 in regions A–C (Figure 9c). Further research is needed to establish if the occurrence of new contact points is similarly distributed versus stroke order over the ocean. The same study found that only 14% of NGC in subsequent strokes had stroke order of 4 or greater. This result is not consistent with the residual percent increase for the higher stroke order events, which is ∼10% for region A and ∼20%–30% for regions B and C.

[42] A visual comparison between Figure 4a and the annualized distribution of total lightning activity shown in Figure 4 in *Christian et al.* [2003] gives a rough independent validation of GLD360's location accuracy and detection efficiency performance. Sharp gradients in flash density common to both plots that follow a land-sea interface, such as along the northeast Brazilian coastline, suggest that GLD360's location accuracy is not heavily impacted by a transition from land to salt water. The band of enhanced flash rates in central Brazil shows 20–30 flashes · km^{-2} · yr^{-1} in *Christian et al.* [2003], and 2.6–5.1 flashes · km^{-2} · yr^{-1} in Figure 4a. Assuming a 3:1 ratio of cloud flashes to ground flashes and assuming GLD360 primarily detects ground flashes, this ratio translates to ∼52%–68% ground flash DE, consistent with previous validation studies.

[43] **Acknowledgments.** The GLD360 and NLDN data sets were provided by Vaisala, Inc. The authors thank Ken Cummins and Phil Krider for their very helpful comments and input on the paper. The authors also thank the two anonymous reviewers for their feedback and suggestions, which helped to make this paper more complete. This work was supported in part by the DARPA NIMBUS program under grant HR0011-10-1-0058 to Stanford University.

References

Barrington-Leigh, C. P., and U. S. Inan (1999), Elves triggered by positive and negative lightning discharges, *Geophys. Res. Lett.*, *26*, 683–686, doi:10.1029/1999GL900059.

Bazelyan, E. M., and M. I. Chichinskiy (2009), Recovery of the parameters of a lightning current pulse from measurements of the electromagnetic field in the far wave zone, *Plasma Phys. Rep.*, *35*, 794–801, doi:10.1134/S1063780X09090086.

Berger, K. (1967), Novel observations on lightning discharges: Results of research on Mount San Salvatore, *J. Franklin Inst.*, *283*, 478–525, doi:10.1016/0016-0032(67)90598-4.

Berger, K. (1975), Parameters of lightning flashes, *Electra*, *41*, 23–37.

Boccippio, D. J., K. L. Cummins, H. J. Christian, and S. J. Goodman (2001), Combined satellite- and surface-based estimation of the intracloud cloud-to-ground lightning ratio over the continental United States, *Mon. Weather Rev.*, *129*, 108–122, doi:10.1175/1520-0493(2001)129<0108:CSASBE>2.0.CO;2.

Borghetti, A., C. Nucci, and M. Paolone (2003), Effect of tall instrumented towers on the statistical distributions of lightning current parameters and its influence on the power system lightning performance assessment, *Eur. Trans. Electr. Power*, *13*, 365–372.

Chen, A. B., et al. (2008), Global distributions and occurrence rates of transient luminous events, *J. Geophys. Res.*, *113*, A08306, doi:10.1029/2008JA013101.

Christian, H. J., et al. (2003), Global frequency and distribution of lightning as observed from space by the Optical Transient Detector, *J. Geophys. Res.*, *108*(D1), 4005, doi:10.1029/2002JD002347.

Cohen, M. B., U. S. Inan, and E. W. Paschal (2010), Sensitive broadband ELF/VLF radio reception with the AWESOME instrument, *IEEE Trans. Geosci. Remote Sens.*, *48*, 3–17, doi:10.1109/TGRS.2009.2028334.

Cooray, V., and N. Theethayi (2007), The striking distance of lightning flashes and the early streamer emission (ESE) hypothesis, *J. Electrostat.*, *65*, 336–341, doi:10.1016/J.ELSTAT.2006.09.006.

Cummins, K. L., and M. J. Murphy (2009), An overview of lightning location systems: History, techniques, and data uses, with and in-depth look at the U.S. NLDN, *IEEE Trans. Electromagn. Compat.*, *51*(3), 499–518, doi:10.1109/TEMC.2009.2023450.

Cummins, K. L., E. P. Krider, and M. D. Malone (1998a), The US national lightning detection network^{TM} and applications of cloud-to-ground lightning data by electric power utilities, *IEEE Trans. Electromagn. Compat.*, *40*(4), 465–480, doi:10.1109/15.736207.

Cummins, K. L., M. J. Murphy, E. A. Bardo, W. L. Hiscox, R. B. Pyle, and A. E. Pifer (1998b), A combined TOA/MDF technology upgrade of the U.S. National Lightning Detection Network, *J. Geophys. Res.*, *103*(D8), 9035–9044, doi:10.1029/98JD00153.

Cummins, K. L., J. A. Cramer, W. A. Brooks, and E. P. Krider (2005), On the effect of land:sea and other Earth surface discontinuities on LLS-inferred lightning parameters, in *VIII International Symposium on Lightning Protection*, pp. 106-111, University of Sao Paulo, Sao Paulo, Brazil.

Cummins, K. L., M. J. Murphy, J. A. Cramer, W. Scheftic, N. Demetriades, and A. Nag (2010), Location accuracy improvements using propagation corrections: A case study of the US National Lightning Detection Network, in *21st International Lightning Detection Conference*, Vaisala, Inc., Tucson, AZ, available at: http://www.vaisala.com/en/events/ildcilmc/Pages/ILDC-2010-Archive.aspx.

Fukunishi, H., Y. Takahashi, M. Kubota, K. Sakanoi, U. S. Inan, and W. A. Lyons (1996), Elves: Lightning-induced transient luminous events in the lower ionosphere, *Geophys. Res. Lett.*, *23*, 2157–2160, doi:10.1029/96GL01979.

Füllekrug, M., C. Price, Y. Yair, and E. R. Williams (2002), Intense oceanic lightning, *Ann. Geophys.*, *20*, 133–137, doi:10.5194/ANGEO-20-133-2002.

Holle, R. L., R. E. López, and B. C. Navarro (2005), Deaths, injuries, and damages from lightning in the United States in the 1890s in comparison with the 1990s, *J. Appl. Meteorol.*, *44*, 1563–1573, doi:10.1175/JAM2287.1.

Inan, U. S., T. F. Bell, and J. V. Rodriguez (1991), Heating and ionization of the lower ionosphere by lightning, *Geophys. Res. Lett.*, *18*, 705–708, doi:10.1029/91GL00364.

Inan, U. S., C. Barrington-Leigh, S. Hansen, V. S. Glukhov, T. F. Bell, and R. Rairden (1997), Rapid lateral expansion of optical luminosity in lightning-induced ionospheric flashes referred to as "elves", *Geophys. Res. Lett.*, *24*, 583–586, doi:10.1029/97GL00404.

Jain, R., and I. Chlamtac (1985), The P2 algorithm for dynamic calculation of quantiles and histograms without storing observations, *Commun. ACM*, *28*, 1076–1085.

Jerauld, J., V. A. Rakov, M. A. Uman, K. J. Rambo, D. M. Jordan, K. L. Cummins, and J. A. Cramer (2005), An evaluation of the performance characteristics of the U.S. National Lightning Detection Network in Florida using rocket-triggered lightning, *J. Geophys. Res.*, *110*, D19106, doi:10.1029/2005JD005924.

Kappenman, J., and D. Van House (1996), Location-centered mitigation of lightning-caused disturbances, *IEEE Comput. Appl. Power*, *9*(3), 36–40, doi:10.1109/67.526852.

Kisacanin, B., S. S. Bhattacharya, and S. Chai (eds.) (2009), *Embedded Computer Vision*, Springer-Verlag, London.

Krider, E. P., R. C. Noggle, and M. A. Uman (1976), A gated, wideband magnetic direction finder for lightning return strokes, *J. Appl. Meteorol.*, *15*, 301–306.

Lehmann, T. M., C. Gonner, and K. Spitzer (1999), Survey: Interpolation methods in medical image processing, *IEEE Trans. Med. Imaging*, *18*, 1049–1075.

LeVine, D. M. (1987), Review of measurements of the RF spectrum of radiation from lightning, *Meteorol. Atmos. Phys.*, *37*, 195–204, doi:10.1007/BF01042441.

Lyons, W. A., M. Uliasz, and T. E. Nelson (1998), Large peak current cloud-to-ground lightning flashes during the summer months in the contiguous United States, *Mon. Weather Rev.*, *126*, 2217–2233, doi:10.1175/1520-0493(1998)126<2217:LPCCTG>2.0.CO;2.

Merceret, F., J. Willett, H. Christian, J. Dye, E. Krider, J. Madura, T. O'Brien, W. Rust, and R. Waltersheid (2010), A history of the lightning launch commit criteria and the lightning advisory panel for America's space program, *NASA Tech. Rep.*, NASA/SP-2010-216283.

Murray, N. D., E. P. Krider, and J. C. Willett (2005), Multiple pulses in *dE*/*dt* and the fine-structure of E during the onset of first return strokes in cloud-to-ocean lightning, *Atmos. Res.*, *76*, 455–480, doi:10.1016/J.ATMOSRES.2004.11.038.

Nag, A., et al. (2011), Evaluation of U.S. National Lightning Detection Network performance characteristics using rocket-triggered lightning data acquired in 2004–2009, *J. Geophys. Res.*, *116*, D02123, doi:10.1029/2010JD014929.

Nucci, C. A., F. Rachidi, M. V. Ianoz, and C. Mazzetti (1993), Lightning-induced voltages on overhead lines, *IEEE Trans. Electromagn. Compat.*, *35*(1), 75–86, doi:10.1109/15.249398.

Orville, R. E., and G. R. Huffines (2001), Cloud-to-ground lightning in the United States: NLDN Results in the first decade, 1989–98, *Mon. Weather Rev.*, *129*, 1179–1193, doi:10.1175/1520-0493(2001)129<1179:CTGLIT>2.0.CO;2.

Orville, R. E., and V. P. Idone (1982), Lightning leader characteristics in the Thunderstorm Research International Program (TRIP), *J. Geophys. Res.*, *87*(C13), 11,177–11,192, doi:10.1029/JC087IC13P11177.

Orville, R. E., G. R. Huffines, W. R. Burrows, and K. L. Cummins (2011), The North American Lightning Detection Network (NALDN)—Analysis of flash data: 2001–09, *Mon. Weather Rev.*, *139*, 1305–1322, doi:10.1175/2010MWR3452.1.

Paolone, M., F. Rachidi, A. Borghetti, C. Nucci, M. Rubinstein, V. Rakov, and M. Uman (2009), Lightning electromagnetic field coupling to overhead lines: Theory, numerical simulations, and experimental validation, *IEEE Trans. Electromagn. Compat.*, *51*(3), 532–547, doi:10.1109/TEMC.2009.2025958.

Poelman, D. R., W. Schulz, and C. Vergeiner (2013), Performance characteristics of distinct lightning detection networks covering Belgium, *J. Atmos. Oceanic Technol.*, *30*, 942–951, doi:http://dx.doi.org/10.1175/JTECH-D-12-00162.1.

Pohjola, H., and A. Mäkelä (2013), The comparison of GLD360 and EUCLID lightning location systems in Europe, *Atmos. Res.*, *123*, 117–128, doi:10.1016/J.ATMOSRES.2012.10.019.

Prentice, S. A., and D. MacKerras (1977), The ratio of cloud to cloud-ground lightning flashes in thunderstorms, *J. Appl. Meteorol.*, *16*, 545–550, doi:10.1175/1520-0450(1977)016<0545:TROCTC>2.0.CO;2.

Rakov, V. A., and M. A. Uman (2003), *Lightning - Physics and Effects*, 698 pp., Cambridge Univ. Press, Cambridge.

Said, R. K., U. S. Inan, and K. L. Cummins (2010), Long-range lightning geolocation using a VLF radio atmospheric waveform bank, *J. Geophys. Res.*, *115*, D23108, doi:10.1029/2010JD013863.

Schoene, J., M. A. Uman, and V. A. Rakov (2010), Return stroke peak current versus charge transfer in rocket-triggered lightning, *J. Geophys. Res.*, *115*, D12107, doi:10.1029/2009JD013066.

Stall, C. A., K. L. Cummins, E. P. Krider, and J. A. Cramer (2009), Detecting multiple ground contacts in cloud-to-ground lightning flashes, *J. Atmos. Terr. Phys.*, *26*, 2392–2402, doi:10.1175/2009JTECHA1278.1.

Stano, G. T., H. E. Fuelberg, and W. P. Roeder (2010), Developing empirical lightning cessation forecast guidance for the Cape Canaveral Air Force Station and Kennedy Space Center, *J. Geophys. Res.*, *115*, D09205, doi:10.1029/2009JD013034.

Thottappillil, R., and M. A. Uman (1993), Comparison of lightning return-stroke models, *J. Geophys. Res.*, *98*, 22,903–22,914, doi:10.1029/93JD02185.

Tyahla, L. J., and R. E. Lopez (1994), Effect of surface conductivity on the peak magnetic field radiated by first return strokes in cloud-to-ground lightning, *J. Geophys. Res.*, *99*, 10,517–10,525.

Uman, M., and E. Krider (1982), A review of natural lightning: Experimental data and modeling, *IEEE Trans. Electromagn. Compat.*, *EMC-24*(2), 79–112, doi:10.1109/TEMC.1982.304006.